Removal of Acid Red 33 from Aqueous Solution Using Nanoscale Zero-Valent Iron Supported on Activated Carbon: Kinetic, Isotherm, Thermodynamic Studies

Seyedi, Maryam Sadat; Sohrabi, Mahmoud Reza; Motiee, Fereshteh*[+]; Mortazavinik, Saeid

Department of Chemistry, North Tehran Branch, Islamic Azad university, Tehran, I.R. IRAN

ABSTRACT: *In this study, zero-valent iron nanoparticles immobilized on activated carbon (nZVI-AC) were synthesized to rapidly remove Acid Red 33 (AR 33) as an azo dye from an aqueous medium. This novel nanocomposite was characterized by Scanning Electron Microscopy (SEM), Energy Dispersive X-ray Spectroscopy (EDS), X-Ray Diffraction (XRD), and Fourier Transform InfraRed (FT-IR)spectroscopy. The effect of experimental variables, including adsorbent dosage, pH, initial concentration of AR 33, and the temperature was studied to select the optimum conditions for maximum removal efficiency. The optimal conditions were achieved at an adsorbent dosage of 0.2 g/L, pH=3, initial dye concentration of 10 mg/L, and a temperature of 313 K. Isotherms and kinetics studies indicated that Langmuir isotherm with regression determination (R^2) of 0.9914 and pseudo-first-order model with R^2=0.9922 fitted well to the experimental data. The calculated thermodynamic parameters such as ΔG°, ΔH°, and ΔS° revealed that the adsorption process was spontaneous and endothermic. The reusability of the nZVI-AC was investigated and it found that this adsorbent had a potential ability to remove AR 33 dye.*

KEYWORDS: *Nano zero-valent iron; Activated carbon; Acid Red 33; Removal.*

INTRODUCTION

Water sources are contaminated by various pollutants such as heavy metal ions, dyes, pesticides, etc., which is one of the most serious worldwide environmental problems. Dyes are used in different industries, including paper, textile, food, pharmaceutical, plastics, and leather, they enter the aquatic environment and make increase pollution. [1,2]. Organic matter present in the dyes makes them resistant to chemical and biological oxidation. [3]. Owing to aromatic rings in most dyes, carcinogenic, mutagenic, and toxic effects have been observed in them. Dye adsorption in plants due to their non-degradation can be a factor for genetic mutations [4]. Dyes interfere with the growth of antibacterials and inhibit the photosynthesis of aquatic plants, as well as increase the Chemical Oxygen Demand (COD) of the aqueous solutions [5]. By discharging a large volume of dyes into the water, aquatic

***** *To whom correspondence should be addressed.*
+ *E-mail*: *f.motei@yahoo.com*
1021-9986/2022/3/821-831 *11/$/6.01*

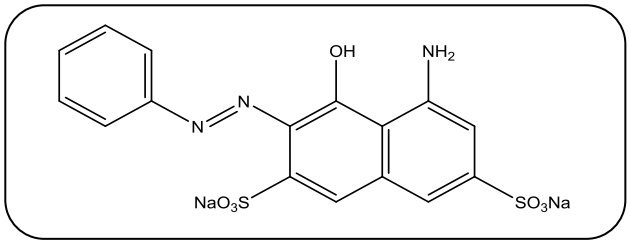

Fig. 1: Chemical structure of AR 33.

environments and human health will be affected [6,7]. Hence, the elimination of these harmful materials should be implemented before releasing them into natural water. 60-70% of the dyes produced worldwide are azo dyes (−N=N−), known as the main source of environmental pollution [8]. Among azo dyes, Acid Red 33 (AR 33) (Fig. 1) is a color additive permitted for mouthwashes, dentifrices, cosmetics, and hair dyes. By coupling diazotized aniline along with 5-amino-4-hydroxy-2,7-naphthalenesulfonic acid in alkaline pH, AR 33 is produced.

It is used in drugs, cosmetics, mouthwashes, toothpaste, and tooth powder [9]. Several methods, including nanofiltration [10], electrochemical [11], photo-electrochemical oxidation [12], coagulation [13], and Fenton oxidation [14] have been utilized to eliminate dyes. The mentioned methods possess some limitations such as complicated operation, high cost, generation of toxic products, and low efficiency [15]. Adsorption methods have some advantages such as simplicity, low-cost, high yield, and adsorbent reusability. Easy operation, insensitivity to harmful compounds, and flexibility are the other benefits of this method. Therefore, it is a suitable treatment technique for the removal of dyes from aquatic media [16-18]. Some of these adsorbents such as activated carbon [19], bentonite [20], multiwall carbon nanotubes [21], alumina nanoparticles [22], synthesized nickel (II) oxide nanoparticles [23], etc. have been used for dye removal.

Nanoscale Zero-Valent Iron (NZVI) has received a lot of attention for removing toxic contaminants due to its nano size, great specific surface area, strong reducing power, degradation ability of the material, and excellent rapid reactivity [24,25]. However, magnetic interactions and high surface energy of iron nanoparticles lead to aggregation and material reactivity is reduced. In order to solve these shortcomings, suitable supports have been developed to stabilize nZVI on their surface [26]. The potential superiority of the use of nZVI in environmental treatment involves enhancing the effectiveness and efficiency of purification corresponding to the soils or ground waters compared to the macro iron particles that are already used [27]. Activated Carbon (AC) has significant properties such as large surface area, high porosity and mechanical strength, and elevated efficiency [28]. Immobilization of the nZVI on the porous surface of AC, reduces the risks of the random release of the nanoparticles into the environment. Stabilized the nZVI on this surface causes the prevent oxidation. Due to the mentioned features, nZVI-AC can be a good adsorbent for dye removal [29]. Therefore, the obtained nanocomposite can adsorb the contaminant and degrade its structure, thereby increasing the removal efficiency of the pollutant occurs.

In this study, nZVI supported by AC was successfully synthesized to rapidly remove AR 33 from an aqueous solution. In the previous research, there was no report about this nano adsorbent for removing AR 33, which has been able to perform the most removal in the shortest time. The prepared nanocomposite was characterized using Scanning Electron Microscopy (SEM), Energy Dispersive X-ray Spectroscopy (EDS), X-Ray Diffraction (XRD), and Fourier Transform InfraRred (FT-IR) spectroscopy. In order to evaluate the performance of dye adsorption on the nano-adsorbent surface, isotherm models were studied. To investigate the speed of reaction and spontaneity of the removal process, kinetic studies and thermodynamic parameters (ΔG°, ΔH°, and ΔS°) were studied. Experimental parameters, including adsorbent dosage, pH, initial dye concentration, and temperature were investigated. Isotherm and kinetics models were studied.

EXPERIMENTAL SECTION

Materials

Acid Red 33 (Color Index: 17200) was procured from Alvan Sabet Co. (Tehran, Iran). Ferric chloride hexahydrate ($FeCl_3.6H_2O$), sodium borohydride ($NaBH_4$), and activated carbon with particle size < 100 µm were procured from Merck (Germany). Sodium hydroxide (NaOH, 0.1 M) and hydrochloric acid (HCl, 0.1 M) were used for pH adjustment.

Synthesis of nZVI-AC nanocomposite

The nZVI-AC nanocomposite was synthesized by adding 5 g of activated carbon to 200 mL of distilled water, then 2 g of iron chloride was added to the solution and the solution was stirred for 5 min. Then 100 mL of 0.3 mM

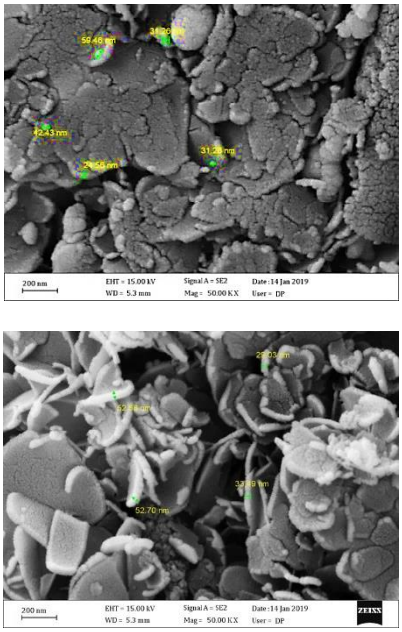

(a)

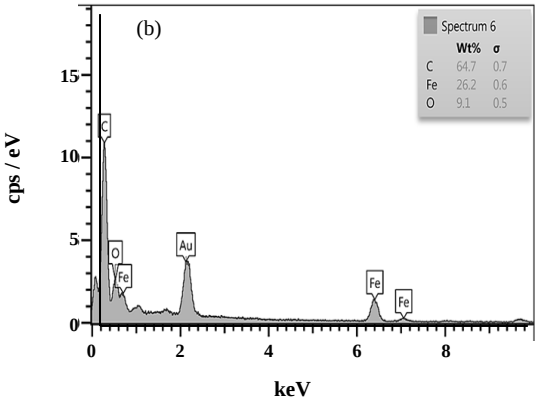

Fig. 2: (a) SEM and (b) EDS of ZVI-AC nanocomposite.

$NaBH_4$ was added to the stirring solution drop by drop. The procedure was done under N_2 atmosphere. The stabilized nZVI particles were separated by filtration and washed 3 times with acetone. It was then stored in a vacuum desiccator. The resulting reaction was [30, 31]:

$$4Fe^{3+}_{(aq)} + 3BH^{-}_{4(aq)} + 9H_2O \rightarrow 4Fe^{0}_{(s)} + 3H_2BO^{-}_{3(aq)} + 12H^{0}_{(s)} + 6H_{2(g)} \quad (1)$$

Characterization techniques of the materials (nZVI-AC)

The morphology and size of nZVI-AC particles were characterized by SEM (FESEM, ZEISS, Sigma VP, Germany), equipped with mapping and WDS detectors. The elemental analysis of the synthesized nanocomposite was studied using EDS (Oxford Instruments, England). XRD analysis of the nZVI-AC was surveyed by Malvern Panalytical (Germany) X-ray diffractometer. FTIR spectra of nZVI-AC composite were determined using Perkin Elmer FTIR spectrophotometer (spectrum GX, USA).

Determination of removal yield

The amount of AR 33 residual was analyzed by a double beam UV–Vis spectrophotometer (Philler Scientific, SU 6100, China) equipped with 1 cm quartz cells at λ_{max}=531 nm. Before determining the concentration of the solution, the nZVI-AC nanocomposite was separated through a centrifuge (ROTINA-380 R, 3000 rpm).

The percentage of AR 33 removal R (%), the adsorption capacity of AR 33 on the nZVI-AC at t min q_t (mg/g), and amount of AR 33 per unit of adsorbent in equilibrium q_e (mg/g) were calculated using Eqs (2), (3), and (4), respectively.

$$R(\%) = \frac{C_0 - C_t}{C_0} \times 100 \quad (2)$$

$$q_t = \frac{(C_0 - C_t)V}{W} \quad (3)$$

$$q_e = \frac{(C_0 - C_e)V}{W} \quad (4)$$

Herein C_0, C_t, and C_e are the initial concentration, concentration at t min, and the equilibrium concentration of AR 33 (mg/L), respectively. V denotes the volume of AR 33 solution (L) and W is the weight of nZVI-AC (g).

RESULTS AND DISCUSSION

Characterization of adsorbent

Fig. 2 (a) reveals the SEM images of nZVI-AC composite. According to the images, the zero-valent iron nanoparticles are not agglomerated by the activated carbon bed and thus uniformLy dispersed and the average particle size of nZVI-AC was uniform and the average particle size of adsorbent was in the range of 24.56-59.46 nm. The results obtained from EDS (Fig. 2 b) confirmed the presence of C, Fe, and O elements on the nanocomposite surface.

Fig. 3 shows the XRD spectra of nZVI/AC. AC has maintained its normal structure. The peak appearing at 2θ equal to 45.55° indicates the presence of nZVI particles

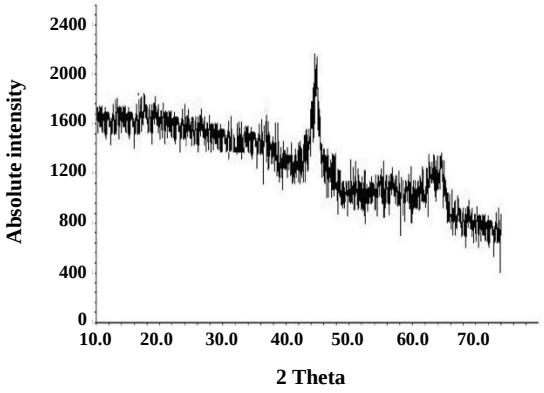

Fig. 3: XRD spectrum of ZVI-AC nanocomposite.

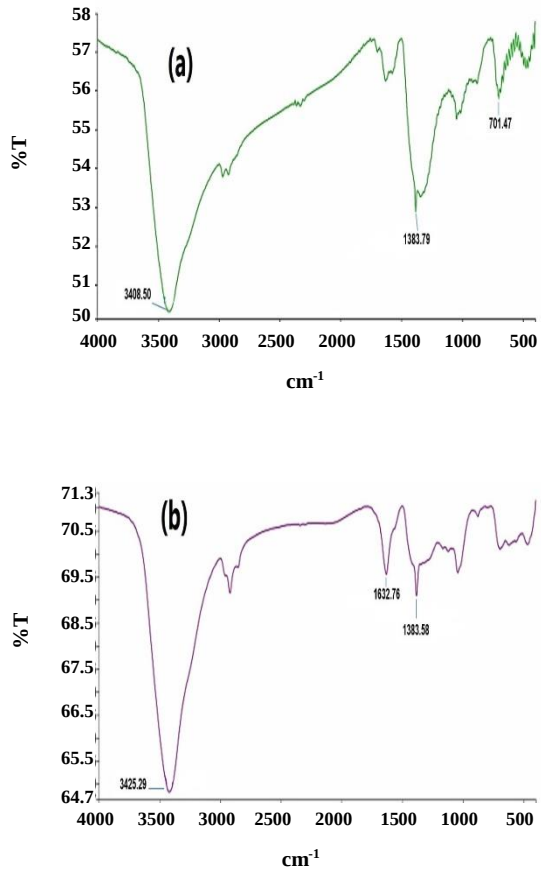

Fig. 4: FTIR spectra of (a) nZVI-AC nanocomposite and (b) nZVI-AC after reaction with AR 33.

inside ACs or inside the network cavities. The appeared peaks in 2θ equal to 30.2°, 35.7°, 43°, 57.2°, and 62.5° are related to Fe_2O_3. Also, peaks in 2θ equal to 44.5°, 64.7°, and 82.8° demonstrate the nZVI [32-34].

FT-IR spectra of nZVI/AC are illustrated in Fig. 4(a). The peaks at 701.47 cm^{-1} are related to Fe_3O_4 and FeO. Also, the peak in the region of 1383.79 cm^{-1} shows the CH_2 and CH_3 groups. In addition, the presence of a wide bond in the 3408.50 cm^{-1} is related to the OH group in H_2O. According to this spectrum, it has been determined that the bonding of magnetic iron nanoparticles to activated carbon has been carried out. Also, Fig. 4(b) displays spectra of nZVI/AC with AR 33. Peaks at 1383.85 and 1632.76 cm^{-1}, are related to the CH_2, CH_3, and activated carbon groups, respectively, as well as the peak in the region of 3425.29 cm^{-1} shows the O H group [32].

Optimization

Effect of adsorbent dosage

The effect of nZVI-AC dosage was studied at different dosages (0.1 to 0.3 g/ l), pH=3, and initial AR 33 concentration of 10 mg/ l at room temperature (25 ºC). By increasing adsorbent dosage, the AR 33 dye removal efficiency was enhanced (Fig. 5a).

The AR 33 removal efficiency increased to 100% with 0.3 g/L of the adsorbent for 8 min. Increasing the nanocomposite dosage provides more surface-active sites to accelerate the initial reaction resulting in more iron ions colliding with dye molecules so, the dye removal efficiency was improved [35].

Effect of pH

In order to assess the effect of pH on the removal percent of AR 33, experiments were accomplished with the adsorbent dosage of 0.2 g/L, initial concentration10 mg/L, and various pHs in the range between 3 to 8 at room temperature (25 ºC). According to Fig. 5 (b), AR 33 removal efficiency increased from 89.72 to 100% by decreasing the solution pH from 8 to 3. The results obtained from experimental data revealed the pH_{ZPC} of nZVI-AC nanocomposite was 6.3. It can be concluded that the positively charged surface of nZVI-AC interacted with the negatively charged sulfuric group related to the AR 33 at pH <pH_{zpc} ≈ 6. Less than a pH of the zero point of charge (pH_{ZPC}), which is equal to 6.3, the surface of adsorption has a positive charge. At pH<3.6 and pH>3.6, the nZVI-AC surface becomes positive and negative, respectively. It can be assumed that at high pH, a large amount of zero iron is changed to iron oxide-hydroxide or iron oxide. Therefore, its activity has decreased [36]. On the other hand,

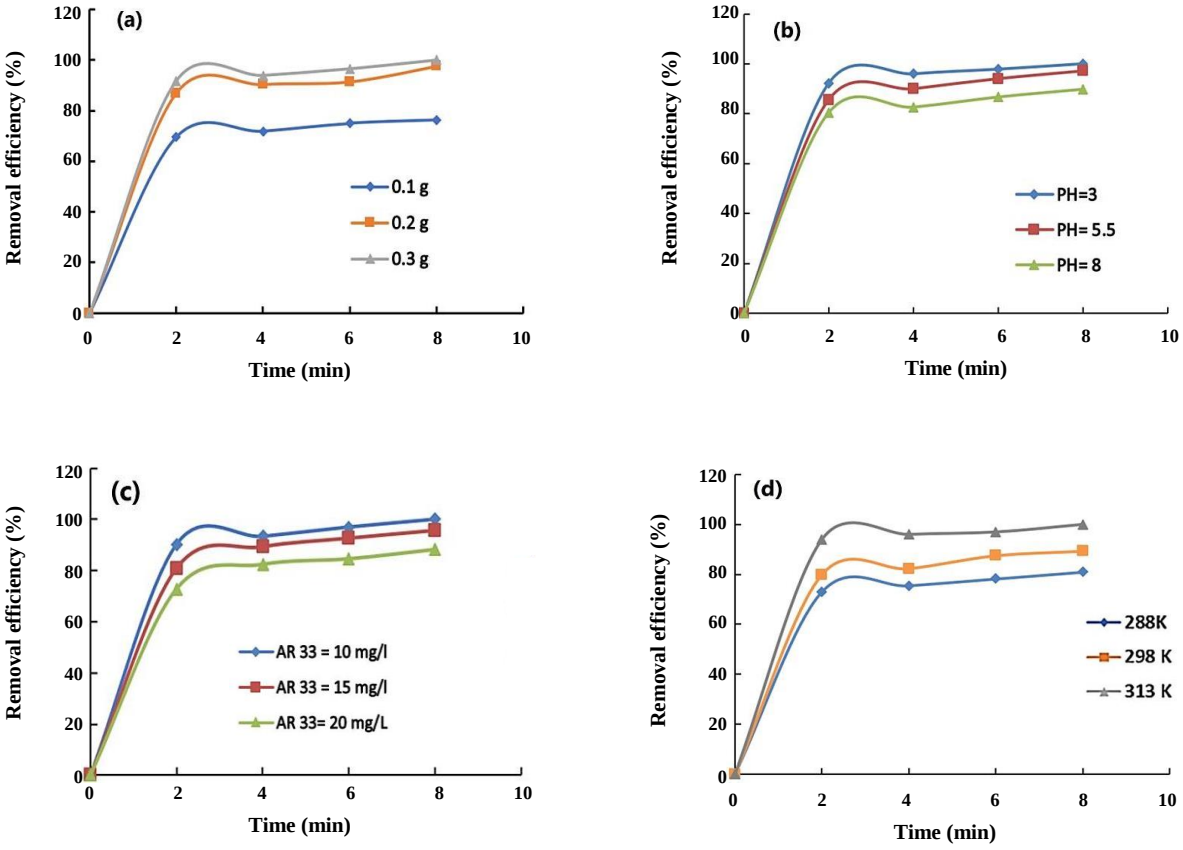

Fig. 5: The effect of (a) adsorbent dosage, (b) pH, (c), initial concentration (d) temperature on the removal of AR 33.

in the acidic environment due to adsorption and hydrogen radical production, the dye degradation process increases. It is most probable that lowering the pH generally increases the H^+ amount which provides the required protons for the reduction process according to the proposed dye reduction reactions (Eqs (5-8)). According to the explanations, the mechanism is as follows [37]:

$$Fe^{\circ} \leftrightarrow Fe^{2+} + 2e^{-} \quad (5)$$

$$2H^{+} + 2e^{-} \leftrightarrow 2H_{ads} \quad (6)$$

$$nH_{ads} \leftrightarrow nH^{+} + ne^{-} \quad (7)$$

$$Dye(Ox.state) + ne^{-} \leftrightarrow Dye(Red.state) \quad (8)$$

Effect of initial dye concentration

The initial concentration of AR 33 in the range of 10 to 20 mg/L was investigated. The other parameters, including pH and adsorbent dosage, were constant at 3 and 0.2 g/L, respectively. By reducing the initial dye concentration from 20 to 10 mg/L, the AR 33 removal efficiency was enhanced from 88.16 to 100% (Fig. 5c) because of the many empty sites of the nano adsorbent in low dye concentration. As shown, more than 70 % of AR 33 was removed within the first 2 min. This indicates the high rate of the contaminant removal reaction and the removal process is complete after 5 min. The short removal time indicates that the nanocomposite was effective in dye removal. At the beginning of the reaction, AR 33 molecules were moved to the nZVI surface due to the strong adsorption and reduction ability of nZVI. The surface of the adsorbent possesses many empty sites and AR 33 can be contacted with available sites on nZVI surface at low concentrations. Therefore, high adsorption was observed by nZVI-AC and the removal efficiency increased [18].

Effect of temperature

The effect of different temperatures (288 to 313 K) on AR 33 removal efficiency was studied at pH=3, the initial

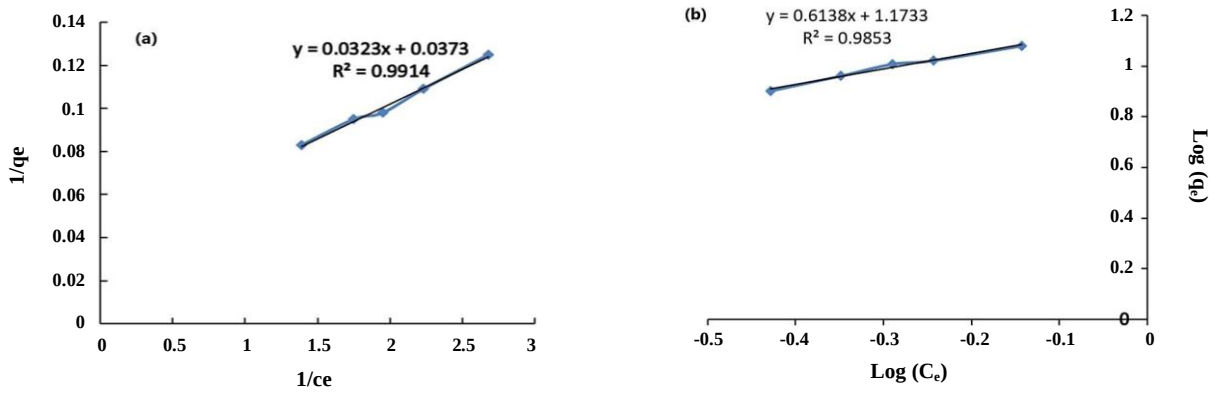

Fig. 6: (a) Langmuir and (b) Freundlich isotherms for removal AR 33.

the concentration of 10 mg/ l, and an adsorbent dosage of 0.2 g/L. As shown in Fig. 5(d), AR 33 removal efficiency was increased from 81 to 100% by increasing the temperature from 288 to 313 K. The results showed that the reaction was endothermic and by increasing the temperature, the process rate was increased.

Adsorption isotherm models

In this study, Langmuir and Freundlich adsorption isotherm models were used to determine the interactive behavior between the adsorbate and adsorbents.

The Langmuir adsorption model expresses that the maximum adsorption is associated with a saturated monolayer of solute molecules on the adsorbent surface. Also, Langmuir isotherm assumes adsorption on homogeneous surfaces. The linear form of the Langmuir isotherm is given by the following equation:

$$\frac{1}{q_e} = \frac{1}{q_m} + \frac{1}{K_L q_m}\frac{1}{C_e} \tag{9}$$

Where q_e (mg/g) is the amount of dye adsorbed at equilibrium and q_m (mg/g) shows the monolayer capacity of the adsorbent. Also, C_e (mg/L) and K_L (L/mg) show the concentration of adsorbate at equilibrium and the Langmuir's adsorption constant, respectively [38,39]. *1/qe* was plotted versus the 1/Ce (Fig. 6a). K_L and q_m were calculated from the intercept and slope of the straight line, respectively.

On the other hand, the Freundlich isotherm, which is assumed multilayer adsorption on heterogeneous surfaces was evaluated. The linear form of the Freundlich adsorption model is defined as follows:

$$Log(q_e) = log K_f + \frac{1}{n} log(C_e) \tag{10}$$

Herein K_f (L/mg) and n (g/L) are related to the adsorption capacity and adsorption intensity, respectively [40]. By plotting log q_e versus log C_e (Fig. 6b), the parameters of this isotherm were obtained.

According to Fig. 6(a) and (b), the correlation determination (R^2) of the Langmuir model was higher than the Freundlich. Hence, the adsorption of AR 33 fitted to Langmuir isotherm, which indicated the monolayer process of adsorption. The calculated parameters related to the Langmuir and Freundlich isotherms are given in Table 1.

Adsorption kinetics studies

The exchanges in dye molecule adsorption were investigated using the pseudo-first-order and pseudo-second-order kinetic models. The pseudo-first-order kinetic model is expressed by Eq (11).

$$log(q_e - q_t) = log q_e - \frac{k_1}{2.303} t \tag{11}$$

Where q_e and q_t (mg/g) are the amount of AR 33 adsorbed at equilibrium and at time t, respectively. Also, k_1 (min^{-1}) is Lagergren rate constant [41]. Calculation of the rate constant, slope, and intercept were implemented by plotting log ($q_e - q_t$) versus time (Fig. 7a).

Besides, the pseudo-second-order kinetic model can be described by Eq (12).

$$\frac{t}{q_t} = \frac{t}{k_2 q_e^t} + \frac{t}{q_e} \tag{12}$$

Table 1: The obtained parameters of isotherm models for AR 33 removal.

Langmuir			Freundlich		
q_m (mg/g)	K_L (l/mg)	R^2	K_f (l/mg)	n	R^2
26.80	1.15	0.9914	14.90	1.62	0.9853

Table 2: The obtained kinetic parameters for AR 33 removal.

pseudo-first order			Pseudo-second order		
k_1 (min^{-1})	q_e (mg g^{-1})	R^2	k_2 (g.mg^{-1}. min^{-1})	q_e (mg g^{-1})	R^2
0.016	4.72	0.9922	0.887	4.95	0.9866

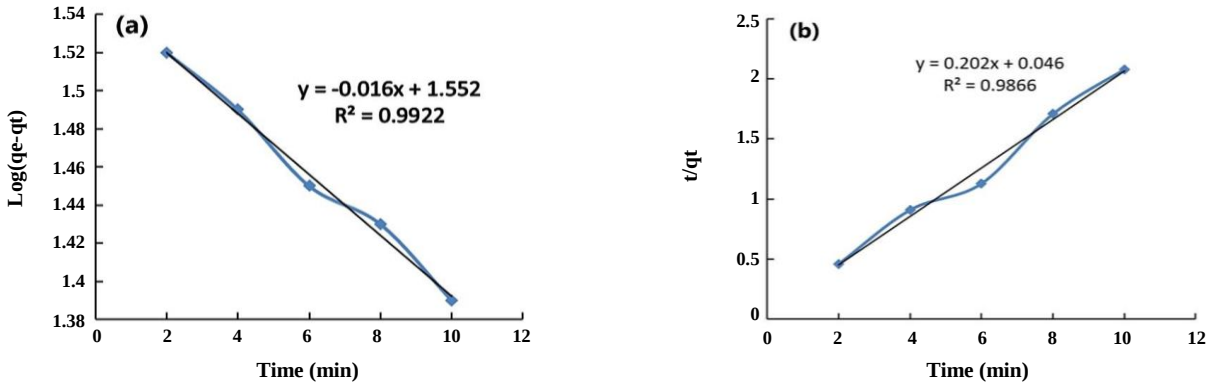

Fig. 7: (a) pseudo-first-order and (b) pseudo-second-order kinetics for removal AR 33.

$$\frac{t}{q_t} = \frac{1}{k_2 q_e^2} + \frac{t}{q_e} \quad (12)$$

Where k_2 (g/mg.min) demonstrates the constant of this model [42]. The q_e, k_2, and R^2 associated with this model were calculated by plotting t/q_t versus time (Fig. 7b).

According to Fig. 7, The high R^2 (0.9922) related to the pseudo-first-order model indicates that the adsorption of dye fitted to this model. The calculated parameters of these models are tabulated in Table 2.

Thermodynamic parameters

Thermodynamic parameters such as Standard free energy change (ΔG°) (kJ/mol), standard enthalpy change (ΔH°) (kJ/mol), and the standard entropy change (ΔS°) (J/mol.K) were determined using the Equations (13) and (14).

$$\Delta G^\circ = \Delta H^\circ - T\Delta S^\circ \quad (13)$$

$$Ln K_c = \frac{\Delta S^\circ}{R} + \frac{\Delta H^\circ}{RT} \quad (14)$$

Where K_c is the adsorption distribution coefficient. T is the absolute temperature (K) and R is the universal gas constant (8.314 J/mol.K) [43,44].

According to Vant Hoff's equation (Eq 14), plotting of Ln k versus 1/T (Fig. 8) was performed. Therefore, ΔH° and ΔS° values were obtained and listed in Table 3. The negative value of ΔG° indicates the spontaneous reaction of AR 33 adsorption onto nZVI-AC nanoparticles. The positive values of ΔH° indicated that the adsorption of AR 33 was endothermic.

Investigating the reusability of adsorbent for AR 33 removal

One of the most important aspects of reducing cost and waste production is adsorbent recycling. Fig. 9 displays the nZVI-AC efficiency for removing AR 33 for 9 repetitions. It can be concluded that the dye removal efficiency decreased from 100 to 44.97% after six cycles. As shown in this figure, the adsorbent has the potential ability after six removal processes.

Table 3: Thermodynamic parameters of AR 33 dye adsorption onto nZVI-AC.

ΔH° (J/mol)	ΔS° (J/(mol.K))	ΔG° (J/mol)		
16984.67	82.72	Temperature (K)		
		288	298	313
		−8908.03	−7667.17	−6839.92

Table 4: Comparison of the proposed adsorbent with other adsorbents.

Adsorbent	Removal efficiency (%)	Pollutant	Time (min)	pH	Temperature (K)	Ref.
Nanozeolite-x	97.60	Crystal violet	6	8	298	[17]
Nano-zero-valent iron	91.03	Direct Red-31	1.83	6	298	[33]
Nano-zero-valent iron	94.57	Direct Brown-2	1.83	6	298	[33]
Granular red mud-supported zero-valent	90.78	Acid Orange 7	120	1	298	[45]
Chitosan particles	84.20	Reactive Red 195	600	4	318	[46]
Modified Kenaf core fiber	97.25	Reactive Orange 16	110	6.5	303	[47]
Zeolite	87.98	Acid Black 26	59.99	4	298	[48]
Zero-valent iron nanoparticles/activated carbon	100.00	Acid Red 33	8	3	313	This study

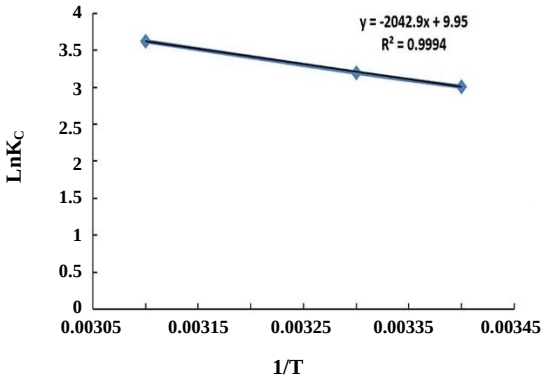

Fig. 8: lnK_c versus 1/T for determination of AR 33 removal reaction enthalpy by nZVI-AC.

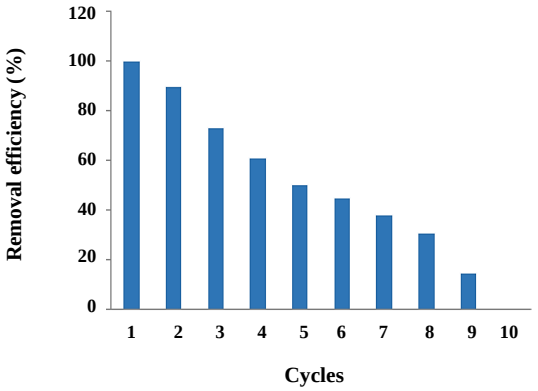

Fig. 8: Reusability of nZVI-AC for removing AR 33.

Comparison with other adsorbents

The removal percentage of nZVI-AC was compared with other adsorbents and the results are summarized in Table 4. It can be seen that the nZVI-AC has excellent removal efficiency and is higher than the other adsorbents. So, its ability is comparable with other adsorbents. In addition to the adsorption process, the feature of the proposed nano absorbent is the degradation ability of pollutant structure. Table 4 shows that the time required to remove high-efficiency pollutants is shorter than the other adsorbents, indicating the high rate of the removal reaction.

CONCLUSIONS

In this study, nanocomposite nZVI-AC was synthesized to rapidly and effectively remove AR 33 dye from an aqueous solution. Characterization methods confirmed the formation of nZVI-AC. Stabilization of nZVI on active carbon increase uniform dispersion followed by increasing active sites, as well as a better stability of iron nanoparticles. Isotherm and kinetics models, also thermodynamic parameters were studied. The removal reaction followed the Langmuir isotherm model. The kinetics reaction revealed that the pseudo-first-order has

a better response. The amount of free energy change showed that the reaction is spontaneous. The effective experimental parameters were optimized and maximum removal was obtained at an adsorbent dosage of 0.2 g/L, pH=3, initial concentration of 10 mg/ L, and temperature of 313 K. In addition, the reusability of nanocomposite represented the ability of adsorbent for AR 33 removal until six cycles without regeneration. The proposed adsorbent has many advantages, such as being cost-effective, and environmentally friendly, and due to adsorption-reduction degradation possesses high-performance removal efficiency, which has great prospects for effective removal of dye from aqueous media.

Received : Sep. 6, 2020 ; Accepted : Dec. 21, 2020

REFERENCES

[1] Basturk E., Alver A., Modeling Azo Dye Removal by Sono-Fenton Processes Using Response Surface Methodology and Artificial Neural Network Approaches, *J. Environ. Manage*., **248**: 109300 (2019).

[2] Nadeem Zafar M., Dar Q., Nawaz F., Effective Adsorptive Removal of Azo Dyes over Spherical ZnO Nanoparticles, *J. Mater. Res. Technol*., **8**: 713-725 (2019).

[3] Yusof N.H., Foo K.Y., Hameed B.H., Hazwan Hussin M., Lee H.K., Sabar S., One-Step Synthesis of Chitosan-Polyethyleneimine with Calcium Chloride as Effective Adsorbent For Acid Red 88 Removal, *Int. J. Biol. Macromol*. (2019).

[4] Pourabadeh A., Baharinikoo L., Nouri A., Mehdizadeh B., Shojaei S., The Optimisation of Operating Parameters of Dye Removal: Application of Designs of Experiments, *Int J Environ Anal Chem*. (2019).

[5] Shojaei S., Shojaei, S., Experimental Design and Modeling of Removal of Acid Green 25 Dye by Nanoscale Zero-Valent Iron, *Euro-Mediterr J. Environ Integr*, **2**: 15 (2017).

[6] Chen Y., Long W., Xu H., Efficient Removal of Acid Red 18 from Aqueous Solution by *In-Situ* Polymerization of Polypyrrole-Chitosan Composites, *J. Mol. Liq*., **287**: 110888 (2019).

[7] Nyoo Putro J., Permatasari Santoso Sh., Edi Soetaredjo F., Ismadji S., Hsu Ju Y., Nanocrystalline Cellulose from Waste Paper: Adsorbent for Azo Dyes Removal, Environmental Nanotechnology. *Monit. Manage*., **12**: 100260 (2019).

[8] Cintra Fernandes N., Barroso Brito L., Goncalves Costa G., FleuryTaveira S., SoaresCunha–Filho M.S., RodriguesOliveira G.A., Neves Marretoa R., Removal of Azo Dye Using Fenton and Fenton-Like Processes: Evaluation of Process Factors by Box–Behnken Design and Ecotoxicity Tests, *Chem. Biol. Interact*., **291**: 47-54 (2018).

[9] Weisz A., Ridge C.D., Mazzola E.P., Itoc Y., Preparative Separation and Identification of novel Subsidiary Colors of the Color Additive D&C Red No. 33 (Acid Red 33) Using Spiralhigh-Speed Counter-Current Chromatography, *J. Chromatogr. A*. **1380**: 120–129 (2015).

[10] Al-Aseeri M., Bu-Ali Q., Haji Sh., Al-Bastaki N., Removal of Acid Red and Sodium Chloride Mixtures From Aqueous Solutions Using Nanofiltration, *Desalination*. **206**: 407–413 (2007).

[11] Anantha M.S., Olivera Sh., Hu Ch., Jayanna B.K., Reddy N., Venkatesh K., Muralidhara H.B., Naidu R., Comparison of the Photocatalytic, Adsorption and Electrochemical Methods for the Removal of Cationic Dyes from Aqueous Solutions, *Environ. Technol. Innovation*, **17**: 100612 (2020).

[12] Mais L., Vacca A., Mascia M., Maria Usai E., Tronci S., Palmas S., Experimental Study on the Optimisation of Azo-Dyes Removal by Photo-Electrochemical Oxidation with TiO_2 Nanotubes, *Chemosphe*re, **248**:125938 (2020).

[13] Kasperchik V.P., Yaskevich A.L., Bil'dyukevich A.V., Wastewater Treatment for Removal of Dyes by Coagulation and Membrane Processes, *Pet. Chem*., **52**: 545–556 (2012).

[14] Hyun Kim T., Park Ch., Yang J., Kim S., Comparison of Disperse and Reactive Dye Removals by Chemical Coagulation and Fenton Oxidation, *J. Hazard. Mater.*, **112:** 95–103 (2004).

[15] Siva Mohan Reddy G., Bhaumik M., Maity A., Sinha Ray S., Removal of Congo Red From Aqueous Solution by Adsorption Using Gum Ghatti and Acrylamide Graft Copolymer Coated with Zero Valent Iron, *Int. J. Biol. Macromol*. **149**: 21-30 (2020).

[16] Wang Sh., Yun Zhai Y., Gao Q., Jun Luo W., Xia H., Gang Zhou Ch., Highly Efficient Removal of Acid Red 18 from Aqueous Solution by Magnetically Retrievable Chitosan/Carbon Nanotube: Batch Study, Isotherms, Kinetics, and Thermodynamics, *J. Chem. Eng. Data*., **59**: 39-51 (2014).

[17] Shojaei S., Ahmadi J., Davoodabadi Farahani M., Mehdizadeh B., Pirkamali M., Removal of Crystal Violet Using Nanozeolite-X from Aqueous Solution: Central Composite Design Optimization Study, *J. Water Environ. Nanotechnol*, **4**: 40-47 (2019).

[18] Mehr H.V., Saffari J., Mohammadi S.Z., Shojaei S., The Removal of Methyl Violet 2B Dye Using Palm Kernel Activated Carbon: Thermodynamic and Kinetics Model, *Int. J. Environ. Sci. Technol*., **17**: 1773–1782 (2020).

[19] Tyagi U., Adsorption of Dyes Using Activated Carbon Derived From Pyrolysis of Vetiveria Zizanioides in a Fixed Bed Reactor, *Groundwater Sustainable Dev*., **10**: 100303 (2020).

[20] Meng B., Guo Q., Men X., Ren Sh., Jin W., Shen B., Modified Bentonite by Polyhedral Oligomeric Silsesquioxane and Quaternary Ammonium Salt and Adsorption Characteristics for Dye, *J. Saudi Chem. Soc*., **24**: 334-344 (2020).

[21] Shabaan O.A., Jahin H.S., Mohamed G.G., Removal of Anionic and Cationic Dyes from Wastewater by Adsorption Using Multiwall Carbon Nanotubes, *Arabian J. Chem*., **13**: 4797–4810 (2020).

[22] Bhargavi R.J., Maheshwari U., Gupta S., Synthesis and Use of Alumina Nanoparticles as an Adsorbent for the Removal of Zn (II) and CBG Dye from Wastewater, *Int. J. Ind. Chem*., **6**: 31–41 (2015).

[23] Baig U., Kashif Uddin M., Gondal M. A., Removal of Hazardous Azo Dye from Water Using Synthetic Nano Adsorbent: Facile Synthesis, Characterization, Adsorption, Regeneration and Design of Experiments, *Colloids Surf. A*., **584**: 124031 (2020).

[24] Su L., Liu Ch., Liang K., Performance Evaluation of Zero-Valent Iron Nanoparticles (NZVI) for High-Concentration H_2S Removal From Biogas at Different Temperatures, *RSC Adv*., **8**: 13798–13805 (2018).

[25] Almeelbi T., Bezbaruah A., Aqueous Phosphate Removal Using Nanoscale Zero-Valent Iron, *J. Nanopart. Res*., **14**: 900 (2012).

[26] Siciliano A., Limonti C., Nanoscopic Zero-Valent Iron Supported on MgO for Lead Removal from Waters, *Water*, **10**: 404-418 (2018).

[27] Stefaniuk M., Oleszczuk P., Sik Ok Y., Review on Nano Zerovalent Iron (nZVI): From Synthesis to Environmental Applications, *Chem. Eng. J*., **287**: 618-632 (2016).

[28] Araujo G.X., Costa da Rocha R.D., Rodrigues M. B., Preparation and Application of Zero Valent Iron Immobilized in Activated Carbon for Removal of Hexavalent Chromium from Synthetic Effluent, *Int. J. Appl. Sci. Technol*., **14**: 1-9 (2019).

[29] Qu G., Kou L., Wang T., Liang D., Hu Sh., Evaluation of Activated Carbon Fiber Supported Nanoscale Zero-Valent Iron for Chromium (VI) Removal from Groundwater in a Permeable Reactive Column, *J. Environ. Manage*., **201**: 378-387 (2017).

[30] Mansouriieh N., Sohrabi M.R., Khosravi M., Optimization of Profenofos Organophosphorus Pesticide Degradation by Zero-Valent Bimetallic Nanoparticles Using Response Surface Methodology, *Arabian J. Chem*., **12**: 2524-2532 (2019).

[31] Pasinszki T., Krebsz M., Synthesis and Application of Zero-Valent Iron Nanoparticles in Water Treatment, Environmental Remediation, Catalysis, and Their Biological Effects, *Nanomaterials*, **10**: 917 (2020).

[32] Sohrabi M. R., Mansouriieh N., Khosravi M., Zolghadr M., Removal of Diazo Dye Direct Red 23 From Aqueous Solution Using Zero-Valent Iron Nanoparticles Immobilized on Multi-Walled Carbon Nanotubes, *Water Sci. Technol*., **71**: 1367–1441 (2015).

[33] Pourabadeh A., Baharinikoo L., Shojaei S., Mehdizadeh B., Davoodabadi Farahani M., Shojaei S., Experimental Design and Modelling of Removal of Dyes Using Nano-Zero-Valent Iron: A Simultaneous Model, *Int. J. Environ. Anal. Chem.* **100**: 1707-1719 (2020).

[34] Shojaei S., Shojaei S., Optimization of Process Variables by the Application of Response Surface Methodology for Dye Removal Using Nanoscale Zero-Valent Iron, *Int. J. Environ. Sci. Technol*., **16**: 4601–4610 (2019).

[35] Jin X., Zhuang Z., Yu B., Chen Zh., Chen Z., Functional Chitosan-Stabilized Nanoscale Zero-Valent Iron Used to Remove Acid Fuchsine with the Assistance of Ultrasound, *Carbohydr. Polym*., **136**: 1085-1090 (2016).

[36] Venkatapathy R., Bessingpas D.G., Canonica S., Bessingpas D.G., Perlinger J.A., Kinetic Models for Trichloroethylene Transformation by Zero-Valent Iron, *Appl. Catal. B.* ,**37**: 139-159 (2002).

[37] Sabouri M.R., Sohrabi M.R., Zeraatkar Moghaddam A., A Novel and Efficient Dyes Degradation Using Bentonite Supported Zero- Valent Iron- Based Nanocomposites, *Chemistry Select*., **5**: 369-378 (2020).

[38] Veloso C.H., Filippov L.O., Filippova I.V., Ouvrard S., Araujo A.C., Adsorption of Polymers onto Iron Oxides: Equilibrium Isotherms, *J. Mater. Res. Technol*., **9**: 779–788 (2020).

[39] Mudzielwana R., Wilson Gitari M., Ndungu P., Performance Evaluation of Surfactant Modified Kaolin clay in As(III) and As(V) Adsorption from Groundwater: Adsorption Kinetics, Isotherms and Thermodynamics, *Heliyon*. **5**: e02756 (2019).

[40] Mondal S., Majumder S.K., Honeycomb-Like Porous Activated Carbon for Efficient Copper (II) Adsorption Synthesized from Natural Source: Kinetic Study and Equilibrium Isotherm Analysis, *J. Environ. Chem. Eng*., **7**: 103236 (2019).

[41] Li Chen X., Li F., Jie Xie X., Zh. Li, Zh., Chen L., Nanoscale Zero-Valent Iron and Chitosan Functionalized Eichhornia Crassipes Biochar for Efficient Hexavalent Chromium Removal, *Int. J. Environ. Res. Public Health*., **16**: 3046-3061 (2019).

[42] Naghizadeh A., Ghafouri M., Synthesis of Low-Cost Nanochitosan from Persian Gulf Shrimp Shell for Efficient Removal of Reactive Blue 29 (RB29) Dye from Aqueous Solution, *Iran. J. Chem. Chem. Eng. (IJCCE)*, **38**: 93-103 (2019).

[43] Naushad M., Abdullah Alqadami A., Abdullah AlOthman Z., Alsohaimi I.H., Algamdi M.S., Aldawsari A.M., Adsorption Kinetics, Isotherm and Reusability Studies for the Removal of Cationic Dye from Aqueous Medium Using Arginine Modified Activated Carbon, *J. Mol. Liq*., **293**: 111442 (2019).

[44] Abdel-Mohsen A.M., Jancar J., Kalina L., Hassan Asaad F., Comparative Study of Chitosan and Silk Fibroin Staple Microfibers on Removal of Chromium (VI): Fabrication, Kinetics and Thermodynamic Studies, *Carbohydr. Polym*., **234**: 115861(2020).

[45] Du Y., Dai M., Cao J., Peng Ch., Ali I., Naz I., Li J., Efficient Removal of Acid Orange 7 Using a Porous Adsorbent-Supported Zero-Valent Iron as a Synergistic Catalyst in Advanced Oxidation Process, *Chemosphere*, **244**: 125522 (2020).

[46] Perez-Calderon J., Santos M.V., Zaritzky N., Reactive RED 195 Dye Removal Using Chitosan Coacervated Particles as Bio-Sorbent: Analysis of Kinetics, Equilibrium and Adsorption Mechanisms, *J. Environ. Chem. Eng*., **6**:6749-6760 (2018).

[47] Kadhim Obaid M., Chuah Abdullah L., Idan I. J., Removal of Reactive Orange 16 Dye from Aqueous Solution by Using Modified Kenaf Core Fiber, *J. Chem*. **2016**: 1-8 (2016).

[48] Shojaei S., Shojaei S., Pirkamali M., Application of Box–Behnken Design Approach for Removal of Acid Black 26 from Aqueous Solution Using Zeolite: Modeling, Optimization, and Study of Interactive Variables, *Water Conserv. Sci. Eng*., **4**: 13–19 (2019).